Genetic screens identified dual roles of microtubule-associated serine threonine kinase and CREB within a single thermosensory neuron in the regulation of *Caenorhabditis elegans* thermotaxis behavior

Shunji Nakano [1,2,*], Airi Nakayama [2,‡], Hiroo Kuroyanagi [2,‡], Riku Yamashiro [2,‡], Yuki Tsukada [1,2], Ikue Mori [1,2,*]

[1]Neuroscience Institute, Graduate School of Science, Nagoya University, Nagoya, Aichi 464-8602, Japan
[2]Division of Natural Science, Department of Biological Science, Graduate School of Science, Nagoya University, Nagoya, Aichi 464-8602, Japan

*Corresponding author: Neuroscience Institute, Graduate School of Science, Nagoya University, Nagoya, Aichi 464-8602, Japan. Email: z48329a@nucc.cc.nagoya-u.ac.jp;
*Corresponding author: Neuroscience Institute, Graduate School of Science, Nagoya University, Nagoya, Aichi 464-8602, Japan. Email: m46920a@nucc.cc.nagoya-u.ac.jp
‡These authors contributed equally to this work.

Abstract

Animals integrate sensory stimuli presented at the past and present, assess the changes in their surroundings and navigate themselves toward preferred environment. Identifying the neural mechanisms of such sensory integration is pivotal to understand how the nervous system generates perception and behavior. Previous studies on thermotaxis behavior of *Caenorhabditis elegans* suggested that a single thermosensory neuron AFD plays an important role in integrating the past and present temperature information and is essential for the neural computation that drives the animal toward the preferred temperature region. However, the molecular mechanisms by which AFD executes this neural function remained elusive. Here we report multiple forward genetic screens to identify genes required for thermotaxis. We reveal that *kin-4*, which encodes the *C. elegans* homolog of microtubule-associated serine threonine kinase, plays dual roles in thermotaxis and can promote both cryophilic and thermophilic drives. We also uncover that a thermophilic defect of mutants for *mec-2*, which encodes a *C. elegans* homolog of stomatin, can be suppressed by a loss-of-function mutation in the gene *crh-1*, encoding a *C. elegans* homolog CREB transcription factor. Expression of *crh-1* in AFD restored the *crh-1*-dependent suppression of the *mec-2* thermotaxis phenotype, indicating that *crh-1* can function in AFD to regulate thermotaxis. Calcium imaging analysis from freely moving animals suggest that *mec-2* and *crh-1* regulate the neuronal activity of the AIY interneuron, a postsynaptic partner of the AFD neuron. Our results suggest that a stomatin family protein can control the dynamics of neural circuitry through the CREB-dependent transcriptional regulation within a sensory neuron.

Keywords: *Caenorhabditis elegans*; thermotaxis; AFD; MAST kinase; stomatin

Introduction

Information processing in the nervous system is essential for animals to survive and reproduce in response to changes in their environments. Research in the past decades have identified basic principles of the neural circuit operation that enable several functions of neural computations such as gain control of sensory stimuli and integration of multiple sensory stimuli (Dunn and Rieke 2006; van Atteveldt *et al.* 2014). Identifying the site of such neural computations and deciphering the molecular and circuit mechanisms thereof are critical steps toward understanding how the nervous system generates perception and behavior.

Integration of sensory stimuli presented at different time points allows the animals to assess the changes in the environment and underlies decision making in the nervous system. Studies of the thermotaxis behavior of the nematode *Caenorhabditis elegans* provides a unique opportunity in which to study the neural mechanism of such computation. The wild-type

animals that have been cultivated at a certain temperature with food migrate toward that cultivation temperature when placed on a thermal gradient (Hedgecock and Russell 1975). Thus, the *C. elegans* nervous system apparently compares the past and the present temperature information and executes the appropriate behavior that drives the animal toward the cultivation temperature (Luo *et al.* 2014; Ikeda *et al.* 2020). Neural circuitry required for thermotaxis has been extensively studied (Mori and Ohshima 1995; Kuhara *et al.* 2008; Beverly *et al.* 2011; Ikeda *et al.* 2020). Central to this circuitry is the thermosensory neurons AFD and its postsynaptic interneurons AIY (White *et al.* 1986; Cook *et al.* 2019). The AFD neurons respond to temperature stimuli and increase intracellular calcium (Ca^{2+}) level upon warming (Kimura *et al.* 2004; Clark *et al.* 2006, 2007; Ramot *et al.* 2008; Takeishi *et al.* 2016; Tsukada *et al.* 2016). The increase in the Ca^{2+} level of the AFD neurons reflects the information of the previous

cultivation temperature and occurs within a temperature range with its lower bound determined by the previous cultivation temperature. Analysis of a primary cultured AFD neurons indicated that the temperature range of the AFD response is an intrinsic property of AFD and does not require the connection to the neural circuits (Kobayashi *et al.* 2016). Recent studies also suggested that in addition to these temperature-evoked Ca^{2+} responses, the AFD neuron modulates its neuronal outputs such that it evokes distinct responses in its postsynaptic neuron AIY (Hawk *et al.* 2018; Nakano *et al.* 2020). Thus, the single AFD neurons integrate the past and present temperature information and execute single-cell computation to achieve thermotaxis behavior. A similar neural operation has been also reported in the circuitry required for salt chemotaxis in *C. elegans* (Sato *et al.* 2021; Hiroki *et al.* 2022), suggesting that a single-cell integration is prevalent in the *C. elegans* nervous system. However, the molecular mechanisms by which the AFD neurons execute this modulation remain elusive.

To further understand the molecular basis of the single-cell computation during *C. elegans* thermotaxis, we here conducted forward genetic screens for mutants defective in thermotaxis. We show that *kin-4*, which encodes the *C. elegans* homolog of microtubule-associated serine threonine (MAST) kinase (Walden and Cowan 1993), plays dual roles in thermotaxis and suggest that KIN-4 is a critical regulator of the single-cell computation within AFD. Our genetic screen also indicated that a thermotaxis defect of a stomatin homolog, *mec-2* (Huang *et al.* 1995; Nakano *et al.* 2020), was suppressed by a loss-of-function mutation in *crh-1*, which encodes the *C. elegans* homolog of CREB transcription factor (Kimura *et al.* 2002). Our results suggest that a stomatin family protein controls the integration of the temperature information in AFD via transcriptional regulation.

Materials and methods

Caenorhabditis elegans strains

The *C. elegans* strains were cultured on NGM plates with the OP50 *Escherichia coli* as food (Brenner 1974). All strains were cultured at 20°C unless otherwise indicated. N2 (Bristol) was used as the wild-type strain. Germline transformation was performed by microinjection as previously described (Mello *et al.* 1991). CRISPR–Cas9-mediated genome editing was performed as previously described (Dickinson *et al.* 2013; Dokshin *et al.* 2018). Mutations, extrachromosomal arrays, integrated transgenes used in this study were described in Supplementary File 1.

Thermotaxis assay

Thermotaxis assays were performed as previously described (Ito *et al.* 2006). Two hermaphrodite animals at the fourth larval stage were placed onto a NGM plate and were allowed to lay eggs. Their F_1 progeny from 2 NGM plates were collected, were washed with NG buffer and were transferred onto the center of a thermotaxis assay plate that had been placed onto a temperature gradient from 17°C to 23°C with the gradient steepness of 0.5°C/cm. The animals were allowed to freely move on the temperature gradient for 1 h. The assay plate was divided into 8 sections along the temperature gradient. The number of animals in each section was counted. Each plot in the figures represents an independent assay result.

Genetic screens for mutants defective in thermotaxis behavior

Wild-type animals were mutagenized by ethyl methanesulfonate (EMS). We incubated L4 hermaphrodites in M9 buffer containing 47 mM EMS for 4 h. The mutagenized animals were recovered onto NGM plates and were allowed to lay eggs. The F_2 progeny were cultivated at 17°C or 23°C and were subjected to thermotaxis assays on a temperature gradient from 17°C to 23°C. Animals that had migrated to the 17°C region when cultivated at 23°C or to the 23°C region when cultivated at 17°C were picked as mutant candidates and were recovered onto NGM plates. We allowed each candidate animal to lay eggs and retested 8–12 lines from each F_2 candidate for thermotaxis behaviors.

To screen for mutations that can suppress the thermophilic phenotype of *mec-2(nj89gf)*, we mutagenized *mec-2(nj89gf)* animals with EMS, and their F_2 progeny cultivated at 20°C were subjected to thermotaxis assay on a temperature gradient from 17°C to 23°C. Animals that had migrated to the 17°C region were picked as mutant candidates, and their progeny were retested for the suppression of the *mec-2(nj89gf)* thermophilic phenotype.

Calcium imaging of the AFD neurons in immobilized animals

We generated animals expressing the calcium indicator YCX1.6 (Madisen *et al.* 2015) in the AFD and AIY neurons. The YCX1.6 in AFD was localized to the nucleus to separate the signals from AFD and AIY. The animals were cultivated at 20°C and were immobilized by placing on a 10% agarose pad with polystyrene beads (Polysciences), which were then covered by a cover slip. The samples were placed on a Peltier device used for the temperature control, and the YFP and CFP images were captured using epi-fluorescent microscope equipped with SOLA light engine (Lumencore) as a light source and were recorded at 1 frame per second with 400 ms exposure. Image processing was performed by MetaMorph software (Molecular Devices), and the fluorescent intensities of YFP and CFP were determined. The ratio change was calculated as $(R_t - R_0)/R_0$, where R_t represents the ratio of YFP to CFP of each frame, and R_0 the mean ratio of the first 10 frames.

Calcium imaging of the AFD and AIY neurons in freely moving animals

Animals expressing YCX1.6 in the AFD nucleus and the AIY neurons were cultivated at 20°C and were placed on a 2% agarose pad and were covered with a cover glass. The samples were placed on a motorized stage (HawkVision Inc.) with a transparent temperature-control device (TOKAI HIT Co. Ltd). We initiated the tracking and recording of the animals as soon as the sample was set and the focus was adjusted. The animals were allowed to freely move on the agarose pad and were subjected to a temperature ramp. The YFP and CFP images were captured at 1 frame per second (30 ms exposure time) for 40 s under epi-fluorescent microscope with SOLA light engine as a light source. The animals were kept under the field of view by controlling the stage movement, which was achieved by real-time analysis of transmitted infrared light images.

The image processing was first performed by DeepLabCut (Mathis *et al.* 2018; Nath *et al.* 2019) to extract the *x*–*y* coordinates of the region of the interest (ROI) for the fluorescent analysis of AFD and AIY. The image analysis was further performed by a custom-written program in MATLAB, and the positions of the ROI predicted by DeepLabCut were manually inspected for each frame. The AFD intensity was analyzed from its nucleus, and the

AIY intensity was measured from a part of its neurite that makes a dorsal turn (White *et al.* 1986; Nakano *et al.* 2020). The ratio of fluorescence intensities (YFP/CFP) was used to calculate the standardized ratio change of AFD and AIY, which was defined as $(R_t - R_{min})/(R_{max} - R_{min})$. The baseline standardized ratio, which was the mean of the standardized ratio values of the frames before the temperature was increased, was subtracted from the standardized ratio change of each frame. We calculated the area under the curve of the AIY standardized ratio change for the entire time window after the temperature stimulus was applied.

Statistics

Normality of the data was assessed by Shapiro–Wilk test. Equal variance among data sets was assessed by Bartlett test. When both normality and equal variance were assumed, we used 1-way analysis of variance (ANOVA) with Tukey–Kramer test or Dunnett test for multiple comparisons. Otherwise, we used Wilcoxon rank sum test or Steel–Dwass test.

Results and discussion

A genetic screen for mutants defective in thermotaxis recovered 21 mutant isolates

To identify genes important for the regulation of thermotaxis, we conducted a genetic screen. We mutagenized the wild-type animals and looked for mutants that migrated toward the 23°C region when cultivated at 17°C or toward the 17°C region when cultivated 23°C (Fig. 1a). From this screen, we isolated 21 mutant strains, which were classified into 3 groups based on their thermotaxis phenotypes: 9 mutants—*nj85, nj89, nj97, nj98, nj102, nj104, nj108, nj111,* and *nj113*—displayed thermophilic phenotypes and migrated toward the higher temperature region when cultivated at 20°C (Fig. 1b: hereafter, the cultivation temperature was set at 20°C unless otherwise indicated); 6 mutants—*nj87, nj90, nj91, nj92, nj94,* and *nj100*—showed athermotactic phenotypes and distributed evenly on the temperature gradient (Fig. 1c); and 6 mutants—*nj86, nj95, nj96, nj107, nj110,* and *nj112*—exhibited cryophilic phenotypes and preferred the colder temperature region (Fig. 1d). We have previously reported that *nj89* is a gain-of-function allele of the gene *mec-2*, which encodes a *C. elegans* homolog of stomatin (Nakano *et al.* 2020) and that *nj90, nj94,* and *nj100* are alleles of *kcc-3*, which encodes a potassium/chloride cotransporter that functions in a glial-like cell (Yoshida *et al.* 2016). In this study, we further characterize some of the thermophilic isolates, as described below.

nj98 and *nj111* are alleles of *pkc-1*

We observed that *nj98* and *nj111* failed to complement each other for their thermotaxis defects. To identify the gene responsible for the thermotaxis defects of these mutants, we mapped *nj111* into a 2.7 Mb interval on chromosome V (Fig. 2a). This region contains the *pkc-1* gene, which encodes a *C. elegans* homolog of protein kinase C-epsilon/eta. Our previous study indicated that *pkc-1*, also known as *ttx-4*, is required for thermotaxis (Okochi *et al.* 2005). We therefore asked whether *nj98* and *nj111* are alleles of *pkc-1*. We conducted DNA sequence analyses of these mutants and identified mutations in *pkc-1*: *nj98* carries a G-to-A transition mutation that is predicted to alter the glycine 1338 codon of *pkc-1c* to an aspartic acid codon; *nj111* is associated with a C-to-T transition mutation that would alter the arginine 80 codon to an opal stop codon (Fig. 2a). Introduction of genomic fragments that harbor the *pkc-1* locus rescued the thermophilic phenotype of *nj98*

animals (Fig. 2b). These results indicated that *nj98* and *nj111* are alleles of *pkc-1*.

nj97 is an allele of *pkc-2*

To identify the gene responsible for the thermophilic defect of *nj97* animals, we mapped *nj97* into a 1.9 Mb region of chromosome X. This region contains the gene *pkc-2*, which encodes a *C. elegans* homolog of protein kinase C beta (Fig. 3a). A previous study indicated that *pkc-2* is required for thermotaxis and that *pkc-2* functions in the AFD thermosensory neuron to regulate thermotaxis (Land and Rubin 2017). We therefore asked whether *nj97* is an allele of *pkc-2*. We identified a G-to-A transition mutation in the *pkc-2* locus of *nj97* animals that is predicted to alter the tryptophan 248 codon of *pkc-2a* to an amber stop codon (Fig. 3b). Introduction of a genomic clone that harbors the *pkc-2* locus rescued the thermophilic phenotype of *nj97* animals (Fig. 3c). These results indicated that *nj97* is an allele of *pkc-2*.

### *nj104* and *nj108* are alleles of *plc-1*

nj104 and *nj108* failed to complement each other for the thermotaxis defect. To identify the gene responsible for their thermotaxis defects, we mapped *nj108* into a 180 kb interval of chromosome X (Fig. 4a). This region contains the *plc-1* locus (Kunitomo *et al.* 2013), which encodes a *C. elegans* homolog of phospholipase C (PLC). PLCs cleaves phosphatidylinositol 4,5-bisphosphate (PIP$_2$) into inositol 1,4,5-triphosplhate (IP$_3$), and diacyl glycerol (DAG), the latter of which is known to act as a second messenger and can bind to and regulate diverse intracellular signaling proteins, including protein kinase C (Brose *et al.* 2004). We conducted DNA sequencing analyses of the *plc-1* locus in *nj104* and *nj108* animals and observed that these mutants carry mutations in *plc-1*: *nj104* is associated with a C-to-T transition mutation that is predicted to alter the glutamine 1,112 codon of *plc-1d* to an ocher stop codon; *nj108* harbors a G-to-A transition mutation in the splice acceptor sequence within the 5th intron of *plc-1d*. Introduction of genomic fragments that harbor the *plc-1* locus partly rescued the thermophilic phenotype of *nj104* animals (Fig. 4b). These observations suggested that *nj104* and *nj108* are alleles of *plc-1*.

Our genetic screen identified 3 genes, *pkc-1, pkc-2,* and *plc-1,* all of which were shown to be involved in the DAG signaling pathway: the PKC-1 and PKC-2 proteins contain the C1 and C2 domains that can bind to DAG (Corbalán-García and Gómez-Fernández 2014), and the PLC-1 protein promotes the production of DAG. Previous studies focusing on the *C. elegans* salt chemotaxis also indicated the importance of the DAG signaling in the ASER chemosensory neurons (Ohno *et al.* 2017). These observations suggest that the DAG signaling plays an important role in the single-cell computation within the *C. elegans* sensory neurons.

nj102 is an allele of *kin-4*

To identify the gene mutated in *nj102* animals, we mapped this mutation into a 300-kb interval of chromosome IV. This region contains the gene *kin-4*, which encodes the *C. elegans* homolog of MAST kinase (Fig. 5a). DNA sequencing analysis revealed that *nj102* animals carry a C-to-T transition mutation that alters the glutamine 1,480 of *kin-4d* to an amber stop codon. We found that the introduction of a genomic clone carrying the *kin-4* locus rescued the thermophilic defect of *nj102* mutants (Fig. 5b). These results indicated that *nj102* is an allele of *kin-4*.

To further characterize the role of the *kin-4* gene in the regulation of thermotaxis, we analyzed other alleles of *kin-4*. As we previously reported (Nakano *et al.* 2020), 2 deletion alleles of *kin-4, tm1049,* and *nj170,* displayed phenotypes distinct from that of
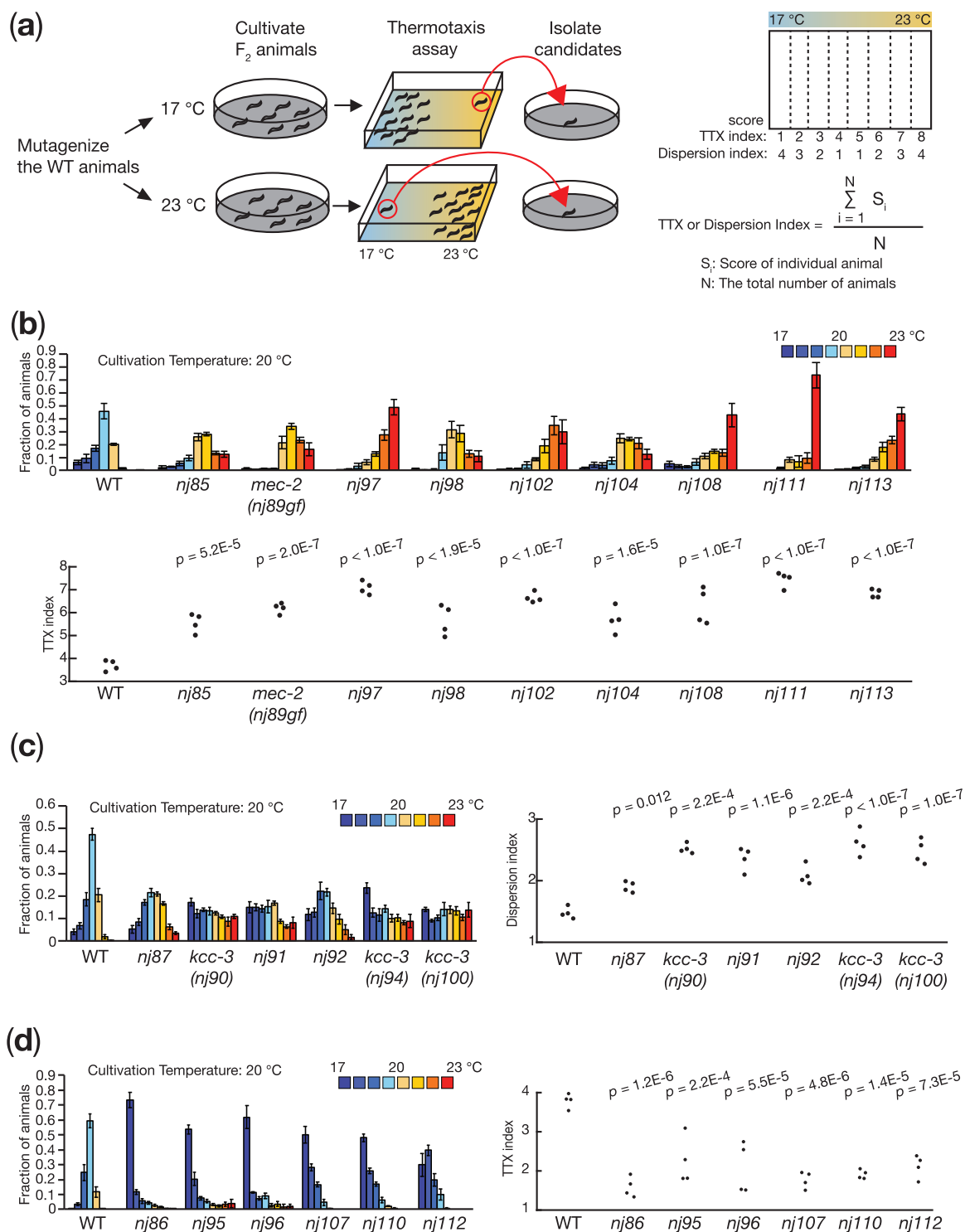
Fig. 1. A forward genetic screen identified mutants defective in *C. elegans* thermotaxis. (a) Schematic of the forward genetic screen and the formulas for TTX and Dispersion indices. We mutagenized the wild-type animals and screened their F$_2$ progeny for mutants defective in thermotaxis. Animals that had migrated to the 23°C or 17°C region after cultivation at 17°C or 23°C, respectively, were isolated as mutant candidates. Thermotaxis behavior was quantified by counting the number of animals in each of the 8 sections along the temperature gradient. We calculated TTX and dispersion indices according to the formulas shown. Thermotaxis behaviors of thermophilic (b), athermotactic (c), and cryophilic (d) mutant isolates. Distributions of the animals in each section of the thermotaxis assay plate are shown as means ± SEM. TTX and dispersion indices are shown as dots. *P*-values were determined by 1-way ANOVA with Tukey–Kramer test.

nj102 animals: *kin-4(tm1049)* and *kin-4(nj170)* mutants displayed bimodal distributions on the temperature gradient, with the majority of animals migrating toward the colder temperature region, while a minor population stayed around the cultivation

temperature region (Fig. 5c). These results indicated that the majority of the *kin-4* null mutant animals display the cryophilic phenotype and that *kin-4* null phenotype is distinct from that of *kin-4(nj102)* animals.

(a)

(b)
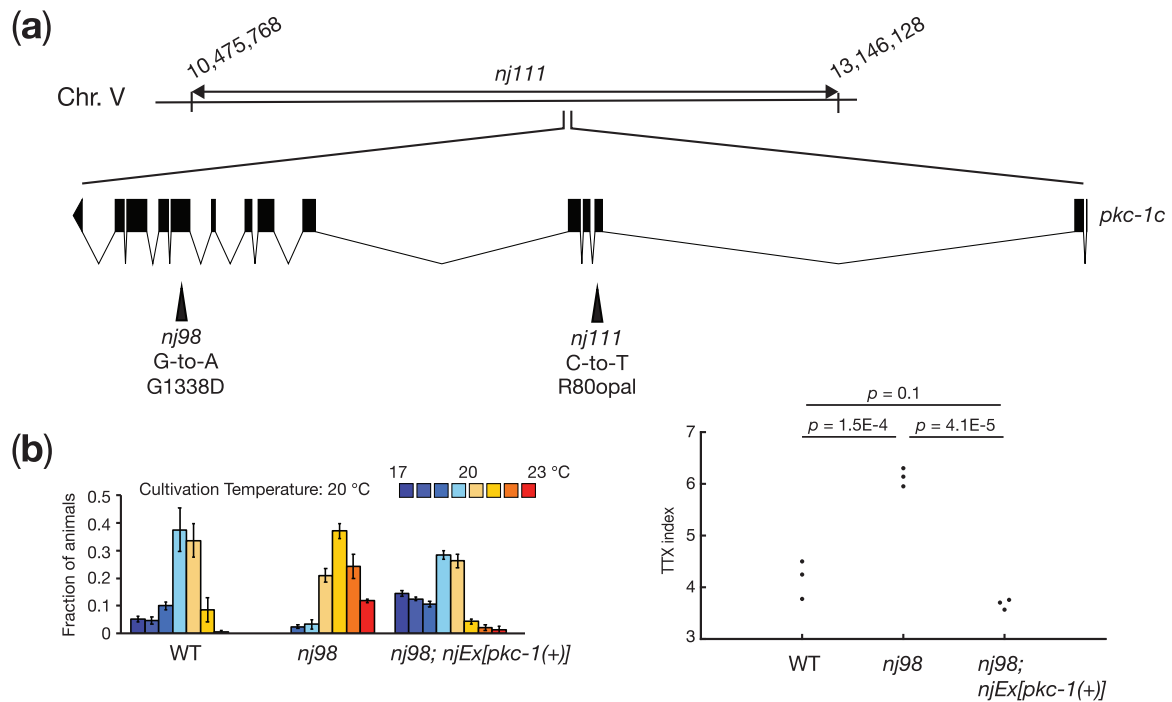
Fig. 2. *nj98* and *nj111* are alleles of *pkc-1*. (a) A chromosomal region to which *nj111* was mapped is indicated. The gene structure of *pkc-1c* is shown. The black boxes indicate exons, and the lines between the black boxes represent introns. Mutations identified in *nj98* and *nj111* are shown. The nucleotides correspond to the sequence in the sense strand. (b) Thermotaxis behaviors of the wild-type, *nj98* and *nj98* carrying genomic fragments containing the *pkc-1* locus. Distributions of animals on the temperature gradient are indicated as means ± SEM. TTX indices are shown as dots. *P*-values were determined by 1-way ANOVA with Tukey–Kramer test.

(a)

(b)
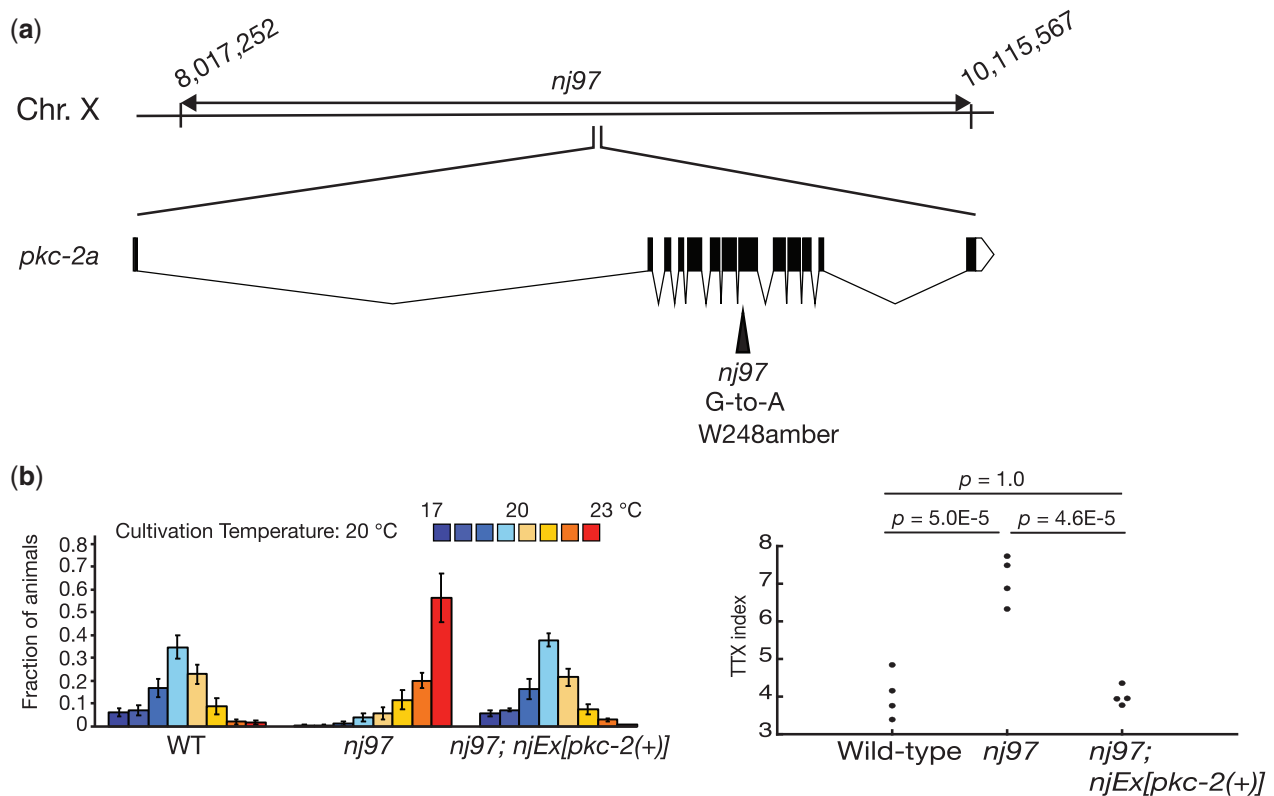
Fig. 3. *nj97* is an allele of *pkc-2*. (a) A chromosomal region to which *nj97* was mapped is indicated. The gene structure of *pkc-2a* is shown. The black boxes indicate exons, and the lines between black boxes represent introns. A mutation identified in *nj97* is shown. (b) Thermotaxis behaviors of the wild-type, *nj97* and *nj97* carrying a genomic clone containing the *pkc-2* locus. Distributions of animals on the temperature gradient are indicated as means ± SEM. TTX indices are shown as dots. *P*-values were determined by 1-way ANOVA with Tukey–Kramer test.
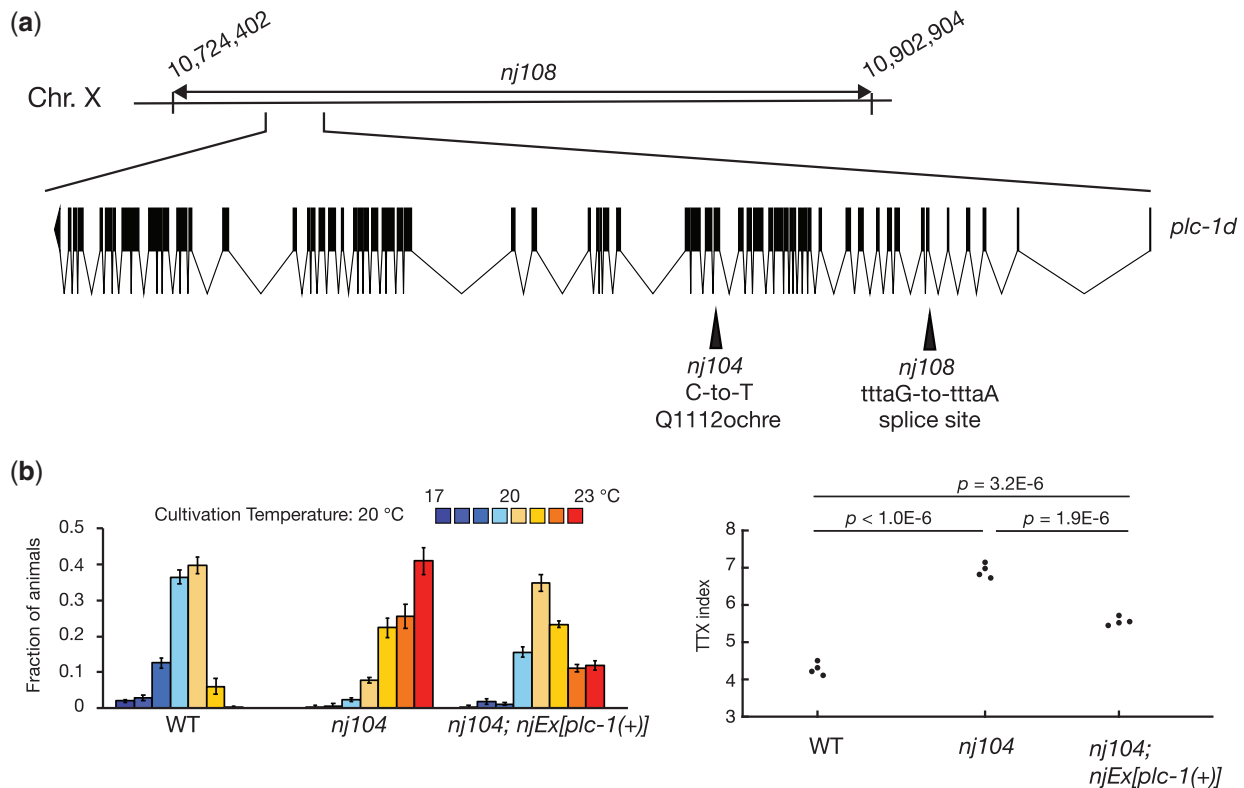
Fig. 4. *nj104* and *nj108* are alleles of *plc-1*. (a) A chromosomal region to which *nj108* was mapped is indicated. The gene structure of *plc-1d* is shown. The black boxes indicated exons, and the lines between the black boxes represent introns. Mutations identified in *nj104* and *nj108* animals are shown. (b) Thermotaxis behaviors of the wild-type, *nj104* and *nj104* carrying genomic fragments containing the *plc-1* locus. Distributions of animals on the temperature gradient are indicated as means ± SEM. TTX indices are shown as dots. *P*-values were determined by 1-way ANOVA with Tukey–Kramer test.

The KIN-4 protein contains 3 major domains: DUF1908 (domain of unknown function), serine-threonine kinase domain and PDZ domain. *nj102* mutants harbor a mutation that would truncate the KIN-4 protein within the PDZ domain (Fig. 5a). To assess whether mutations that would eliminate the PDZ domain from the KIN-4 protein could cause the thermophilic phenotype similar to that of *kin-4(nj102)*, we generated another deletion allele of *kin-4, nj171*. *kin-4(nj171)* removes a part of the coding sequence of KIN-4 polypeptide that corresponds to the PDZ domain and its carboxy-terminal end (Fig. 5a). We found that *kin-4(nj171)* displayed a thermophilic phenotype similar to that of *kin-4(nj102)*. These results suggested that mutations that would eliminate the PDZ domain and C-terminal end of KIN-4 result in thermophilic phenotypes.

kin-4(nj102) is likely a reduction-of-function mutation

To further characterize the nature of the *kin-4(nj102)* allele, we examined the thermotaxis phenotypes of a series of trans-heterozygotes as well as transgenic lines. First, both *nj102/+* and *tm1049/+* heterozygous animals showed the wild-type phenotype (Fig. 5d), indicating that *nj102* and *tm1049* cause recessive phenotypes. To ask whether *kin-4(nj102)* causes a gain-of-function mutation, we injected a genomic clone containing the *kin-4(+)* or *kin-4(nj102)* gene into the wild-type animals. Neither clone affected the thermotaxis phenotype (Fig. 5e), suggesting that *nj102* is not a gain-of-function mutation. When we examined the trans-heterozygotes of *nj102/tm1049*, these animals displayed a thermophilic phenotype similar to that of *nj102* animals (Fig. 5d).

These observations suggested that *nj102* might be a reduction-of-function mutation. We therefore asked whether introduction of the *kin-4(nj102)* genomic clone into a *kin-4(null)* background can alter the thermotaxis phenotype. While introduction of the *kin-4(+)* clone rescued the thermotaxis defect of the *kin-4(tm1049)* animals, *kin-4(tm1049)* animals carrying the *kin-4(nj102)* clone displayed a thermophilic phenotype (Fig. 5f). In contrast, introduction of the *kin-4(tm1049)* genomic clone into *kin-4(nj102)* animals did not affect the thermotaxis phenotype (Fig. 5b). These results suggested that *kin-4(nj102)* is a reduction-of-function mutation.

Our results indicated that *kin-4* can be mutated to cause either a thermophilic or a cryophilic phenotype, suggesting that *kin-4* plays dual roles in regulating thermotaxis, with one activity promoting a thermophilic drive and the other a cryophilic movement. That the *kin-4* null phenotype displayed a bimodal distribution on the temperature gradient is consistent with this notion. Our previous study showed that the AFD-specific expression of a wild-type *kin-4* cDNA rescued the *kin-4* null phenotype (Nakano *et al.* 2020). These observations support that KIN-4 exerts these opposing thermophilic and cryophilic controls within the AFD neurons and suggest that *kin-4* would be a master regulator of single-cell computation by the AFD neuron.

What is the nature of the allele of *kin-4* that causes a thermophilic phenotype? Although the gene dosage analysis of *kin-4* suggested that *kin-4(nj102)* would be a reduction-of-function mutation, *kin-4(nj102)* might not be a simple reduction of function mutation, since heterozygous animals of a *kin-4* null mutation, *kin-4(tm1049Δ)*, showed the wild-type phenotype (Fig. 5d). Our observations indicated that both thermophilic alleles of
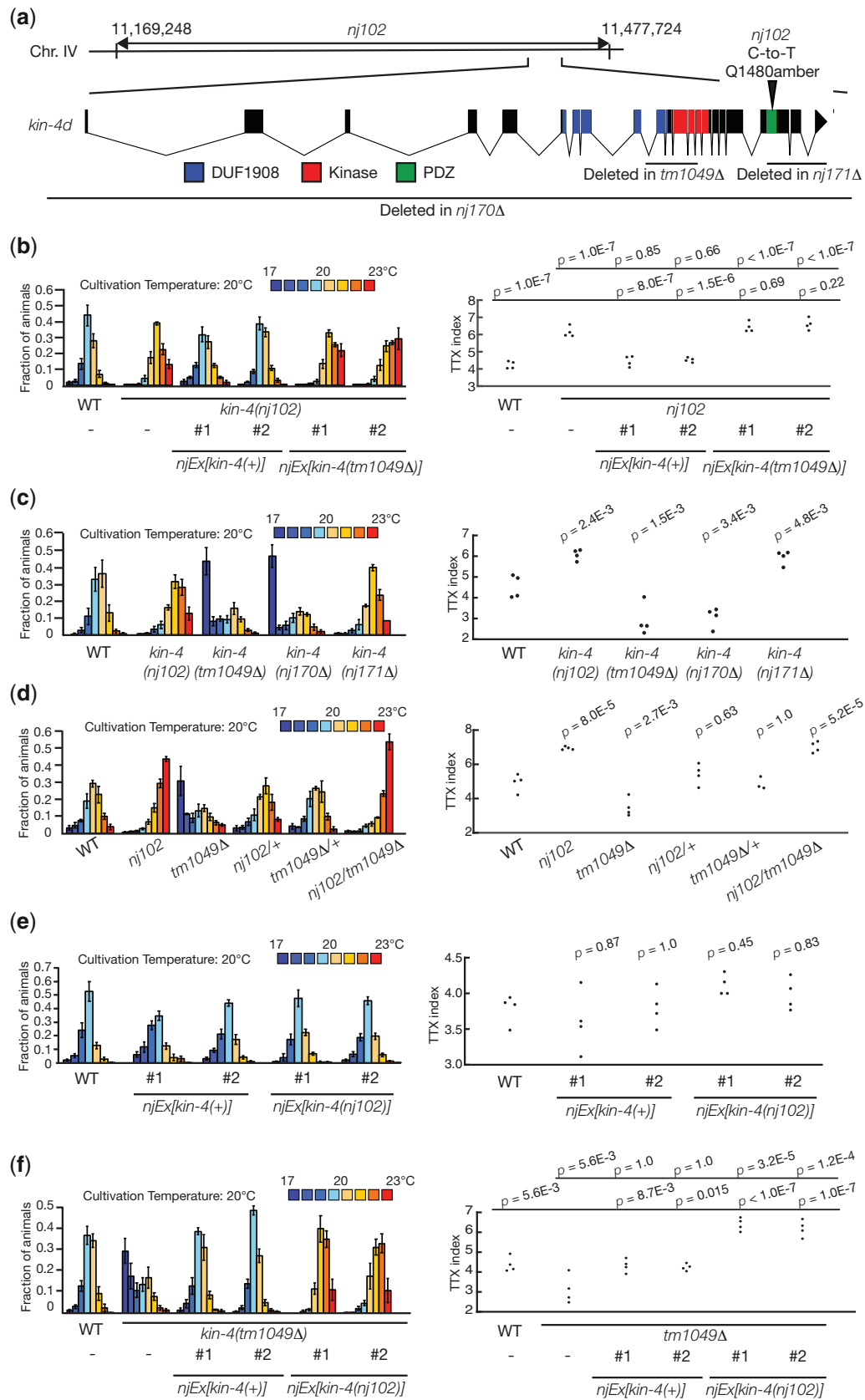
Fig. 5. *nj102* is an allele of *kin-4*. (a) A chromosomal region to which *nj102* was mapped is indicated. The gene structure of *kin-4d* is shown. The boxes indicate exons, and the lines represent introns. The colored boxes denote the coding sequences corresponding to the DUF1908, the kinase and the PDZ domains. Mutations associated with each mutant are shown. Thermotaxis behaviors of *kin-4* mutants. Distributions on the temperature gradients are shown as means ± SEM. TTX indices are indicated as dots. P-values were determined by 1-way ANOVA with Tukey–Kramer tests in (b), (d), (e), and (f), and by 1-way ANOVA with Dunnett test in (c).

kin-4, nj102, and *nj171Δ,* are predicted to remove the PDZ domain from the KIN-4 protein. These results raise the possibility that the PDZ domain of KIN-4 is specifically engaged in the KIN-4 cryophilic activity but is dispensable for its thermophilic drive. We speculate that thermophilic alleles of *kin-4* might result from elimination of the PDZ domain, which causes the reduction specifically in the thermophilic activity of *kin-4* while maintaining the cryophilic activity. Since the PDZ domain is known to be involved in protein–protein interactions, it would be important to determine the interaction partner of KIN-4 through its PDZ domain (An *et al.* 2019). Such analysis might uncover the molecular basis underlying the dual roles of KIN-4 in the AFD thermosensory neurons for the regulation of thermotaxis.

A genetic screen for suppressors of *mec-2(nj89gf)*

Among the thermophilic mutants we had isolated, we have previously shown that *nj89* is a gain-of-function allele of the gene *mec-2* (Nakano *et al.* 2020), which encodes a *C. elegans* homolog of stomatin (Huang *et al.* 1995). We showed that *mec-2* functions in the AFD thermosensory neurons to regulate thermotaxis and that the *mec-2(nj89gf)* mutation affected the neural activity of the AIY interneuron (Nakano *et al.* 2020), which is directly innervated by the AFD thermosensory neurons (White *et al.* 1986; Cook *et al.* 2019). However, the molecular mechanisms by which MEC-2 regulates the AIY neural activity remained elusive.

To further understand the mechanisms by which *mec-2* controls the AIY neural activity and consequently thermotaxis behavior, we conducted another genetic screen to look for mutations that can suppress the thermophilic phenotype of *mec-2(nj89gf)*. We mutagenized *mec-2(nj89gf)* animals and looked for animals that displayed cryophilic phenotypes (Fig. 6a). From this screen, we isolated 13 mutations—*nj254, nj255, nj256, nj257, nj260, nj262, nj263, nj267, nj268, nj269, nj270, nj271,* and *nj274*—that altered the *mec-2(nj89gf)* phenotype. We have previously shown that *nj271* and *nj274* are alleles of *dgk-1,* which encodes a diacylglycerol kinase. *dgk-1* also functions in the AFD thermosensory neurons and affects the neuronal response of the AIY interneuron (Nakano *et al.* 2020).

nj260 and *nj263* are alleles of *ttx-3*

Amongst the isolates we recovered from the *mec-2(nj89gf)* suppressor screen, we observed that *nj260* and *nj263* failed to complement each other. We mapped *nj260* mutation into chromosome X and found that *nj260* carries a mutation in the gene *ttx-3,* which encodes a LIM homeodomain transcription factor required for the cell fate specification of the AIY interneuron (Hobert *et al.* 1997). *nj260* animals are associated with a C-to-T transition mutation that alters the proline 371 codon of *ttx-3a* into a serine codon (Fig. 7a). We could not identify a mutation in the *ttx-3* locus of *nj263.* We attempted to amplify the *ttx-3* locus from *nj263* by polymerase chain reaction (PCR) with multiple primer sets but could not obtain PCR fragments. To assess whether *nj263* is an allele of *ttx-3,* we introduced a genomic PCR product containing the *ttx-3* locus into *mec-2(nj89gf) nj263* animals and observed that the transgenic animals at least partly reverted to the thermophilic phenotype (Fig. 7b). These results indicated that *nj260* and *nj263* are alleles of *ttx-3.* We speculate that *nj263* might carry a complex chromosomal rearrangement that involves the *ttx-3* locus. That loss of *ttx-3* function suppresses the thermophilic defect of *mec-2(nj89gf)* is consistent with our previous observation that *mec-2(nj89gf)* affects thermotaxis through the regulation of the AIY neural activity (Nakano *et al.* 2020).

Loss of *crh-1* function can suppress the thermotaxis defect of *mec-2(nj89gf)*

To identify the gene responsible for *nj257,* we first outcrossed *mec-2(nj89gf); nj257* animals and isolated *nj257* in an *mec-2(+)* background by following the activity that causes the cryophilic phenotype. Using this *nj257* mutant strain, we mapped the mutation into a 45-kb interval of chromosome III (Fig. 8a). This region contains the gene *crh-1,* which encodes a *C. elegans* homolog of CREB transcription factor (Kimura *et al.* 2002; Chen *et al.* 2016). We previously showed that *crh-1* is required for thermotaxis and that *crh-1* functions in the AFD thermosensory neurons to regulate thermotaxis (Nishida *et al.* 2011). DNA sequencing analysis of *nj257* animals identified a G-to-A transition mutation that is predicted to alter the arginine 282 codon of *crh-1a* to a histidine codon (Fig. 8a). A pan-neuronal expression of a *crh-1* cDNA using an *unc-14* promoter rescued the cryophilic defect of *nj257* animals (Fig. 8b). We also generated a deletion allele of *crh-1, nj366,* which is predicted to eliminate the entire DNA binding domain of CRH-1 and is thus likely a null allele of *crh-1.* Like *nj257, crh-1(nj366)* displayed a cryophilic phenotype (Fig. 8c). We also confirmed that *crh-1(tz2),* another deletion allele of *crh-1* (Kimura *et al.* 2002), showed a cryophilic phenotype similar to those observed in *crh-1(nj257)* and *crh-1(nj366)* (Fig. 8c). These results established that *nj257* is an allele of *crh-1* and that loss of *crh-1* function can suppress the thermophilic defect of *mec-2(nj89gf).*

To identify the site of *crh-1* action for the suppression of the thermophilic phenotype conferred by *mec-2(nj89gf),* we conducted a cell-specific rescue experiment. We expressed a *crh-1* cDNA specifically in the AFD or the AIY neurons of *crh-1(nj257); mec-2(nj89gf)* animals and observed that animals expressing *crh-1* in AFD reverted to the thermophilic phenotype, while animals expressing *crh-1* in AIY did not (Fig. 8d). We note that the thermotaxis phenotype of *crh-1(nj257); mec-2(nj89gf)* animal was not completely rescued by the expression of *crh-1* in AFD, suggesting that *crh-1* might also function in a cell(s) other than the AFD neuron. These results indicated that loss of *crh-1* function in AFD can suppress the thermotaxis defect of *mec-2(nj89gf)* and suggested that *crh-1* acts downstream of, or in parallel to, *mec-2* in AFD to regulate thermotaxis.

## *crh-1(nj257)* suppressed the defect of the AIY calcium response of *mec-2(nj89gf)*

We previously showed that the AIY neurons exhibit bidirectional neural responses that correlate with the valence of thermal stimuli: AIY is excited when temperature is increased toward the cultivation temperature, while AIY is inhibited when temperature is increased away from the cultivation temperature. While the temperature-evoked Ca^{2+} responses in the AFD thermosensory neurons are normal in *mec-2(nj89gf)* mutants, they showed a defect in this bidirectional AIY response. The AIY neurons of *mec-2(nj89gf)* animals displayed excitatory responses even when temperature was increased away from the cultivation temperature (Nakano *et al.* 2020).

To investigate the neural mechanisms underlying the *crh-1*-dependent suppression of *mec-2(gf),* we conducted Ca^{2+} imaging experiments. We first examined temperature-evoked Ca^{2+} responses of the AFD thermosensory neurons in immobilized animals. The AFD neurons respond to warming stimuli by increasing the intracellular Ca^{2+} level (Kimura *et al.* 2004; Clark *et al.* 2006; Ramot *et al.* 2008; Kobayashi *et al.* 2016; Takeishi *et al.* 2016; Tsukada *et al.* 2016). We previously showed that the Ca^{2+} responses of the AFD neuron in *mec-2(nj89gf)* animals were
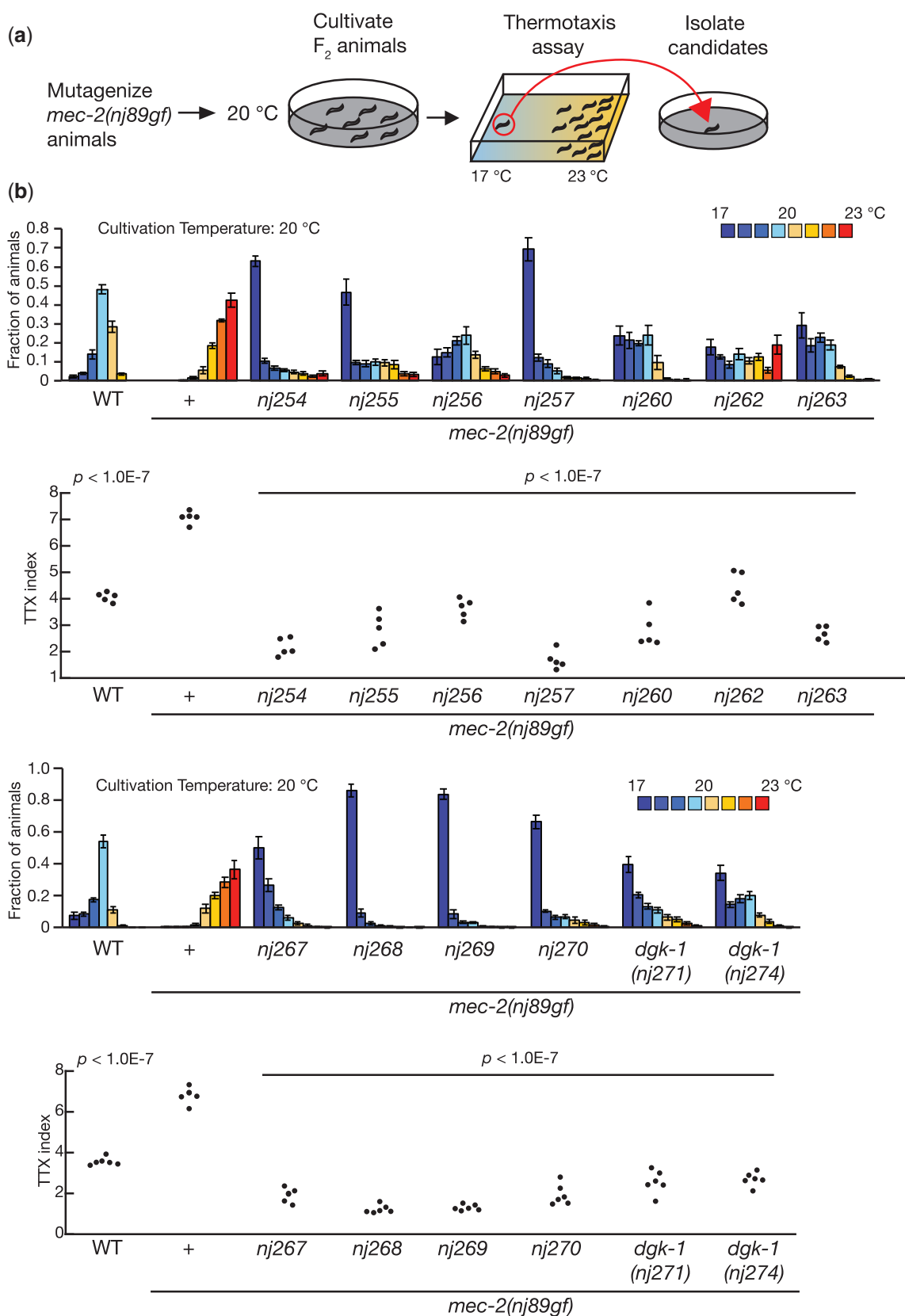
Fig. 6. A genetic screen identified mutations that suppressed the thermophilic defect of *mec-2(nj89gf)*. (a) Schematic of the genetic screen. We mutagenized *mec-2(nj89gf)* animals, and their F$_2$ progeny cultivated at 20°C were subjected to thermotaxis assays. Animals that had migrated toward the 17°C region were isolated as mutant candidates. (b–c) Thermotaxis behaviors of mutant strains isolated from the *mec-2(nj89gf)* suppressor screen. Distributions of animals on the temperature gradients were shown as means ± SEM. TTX indices were indicated as dots. P-values were determined by 1-way ANOVA with Tukey–Kramer test. P-values indicate the comparison of the wild-type and each suppressor isolates to *mec-2(nj89gf)*.
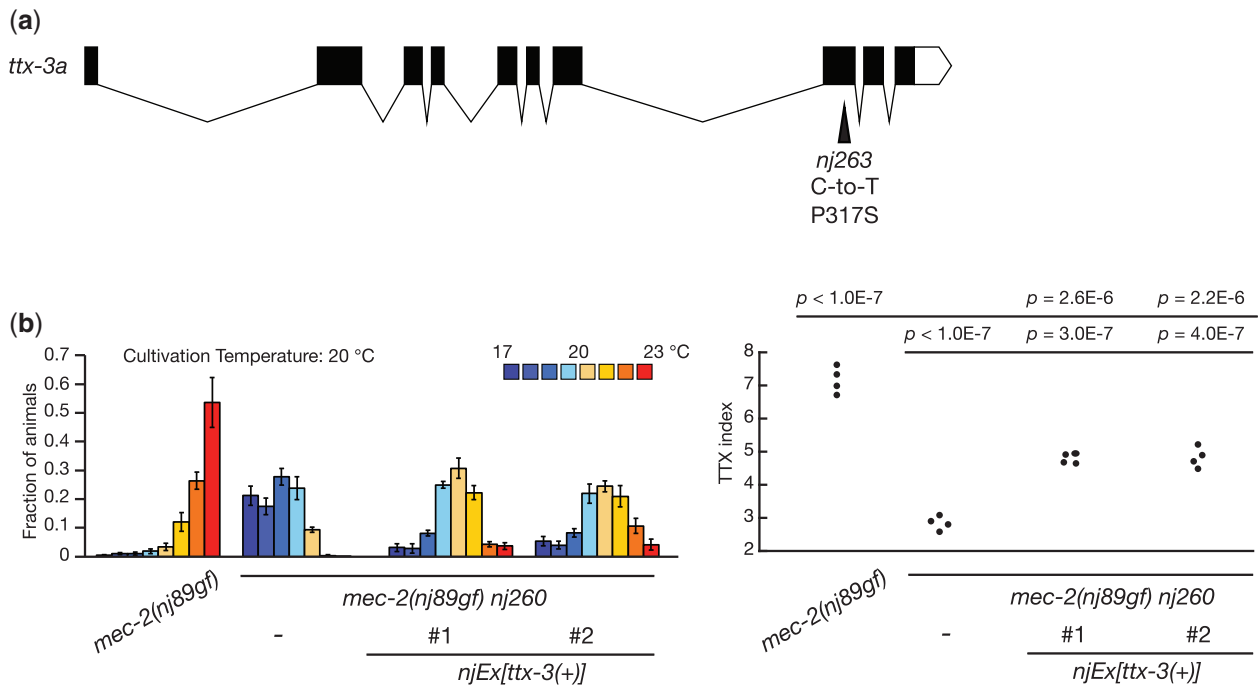
Fig. 7. Mutations in *ttx-3* suppressed the thermophilic defect of *mec-2(nj89gf)*. (a) A gene structure of *ttx-3a* and a mutation found in *nj263* are shown. The black boxes indicate exons, the white box untranslated sequence, and the lines introns. (b) Thermotaxis behaviors of *mec-2(nj89gf)* and *mec-2(nj89gf) nj260* animals with or without a transgene containing a genomic fragment of the *ttx-3* locus. Distributions of animals on the temperature gradients were shown as means ± SEM. TTX indices were indicated as dots. P-values were determined by 1-way ANOVA with Tukey–Kramer test.

indistinguishable from that of the wild-type animals (Nakano *et al.* 2020). When *crh-1(nj257); mec-2(nj89gf)* animals were subjected to temperature ramps, the AFD neurons increased the Ca^{2+} levels similarly to those observed in *mec-2(nj89gf)* animals (Fig. 9a). These results indicate that *crh-1* affects a process downstream of the Ca^{2+} influx in the AFD neurons to suppress the thermotaxis phenotype of *mec-2(nj89gf)*.

We next asked whether *crh-1* regulates the neuronal activity of the AIY interneuron. Since physical immobilization can cause the prolongation of the reversal state in the nervous system (Kato *et al.* 2015), and the AIY neural activity is likely influenced by the motor states of the animal (Li *et al.* 2014; Luo *et al.* 2014), we conducted the imaging from freely moving animals (see Nakano *et al.* 2020 for further discussion). We cultivated animals at 20°C and conducted simultaneous Ca^{2+} imaging of the AFD and AIY neurons from freely moving animals. We subjected the animals to a temperature ramp that increases from 20.2°C to 21.2°C. As previously reported (Nakano *et al.* 2020), the majority of the wild-type AIY neurons displayed inhibitory responses under this condition, while the AIY neurons of *mec-2(nj89gf)* animals predominantly exhibited excitatory responses (Fig. 9b). We observed that a significant fraction of the AIY neurons from *crh-1(nj257); mec-2(nj89gf)* animals displayed inhibitory responses (Fig. 9b). The AFD neurons from both *mec-2(nj89gf)* and *crh-1(nj257); mec-2(nj89gf)* animals showed increases in the Ca^{2+} concentrations upon the warming stimuli. These results suggest that *crh-1* functions in the AFD neurons and regulates the bidirectional responses of the AIY interneurons to regulate thermotaxis.

Our previous study indicated that *crh-1* controls the excitability of the AFD thermosensory neurons in response to certain

thermal stimuli (Nishida *et al.* 2011). Our observations indicated that in addition to this role in regulating the AFD neural activity, *crh-1* controls the neuronal outputs from AFD, thereby governing the bidirectional AIY activity. We suggest that *crh-1* might regulate transcription of a set of genes in AFD, some of which adjust the excitability of the AFD neurons while others control the AFD neuronal output to its postsynaptic neurons AIY. Our results together with our previous observations thus highlight the dual roles of *crh-1* within the AFD neurons for the regulation of thermotaxis.

Our results also suggested that *mec-2* could act upstream of *crh-1* in the AFD thermosensory neurons to regulate thermotaxis. Since *crh-1* is a transcriptional regulator, these observations raised a possibility that *mec-2* would regulate thermotaxis by controlling transcription of genes within AFD that either directly or indirectly affect the neuronal outputs from the AFD neurons. Previous studies indicated that when the cultivation temperature was shifted, the wild-type animals required certain time to adjust their thermotaxis behavior (Hedgecock and Russell 1975; Mohri *et al.* 2005; Aoki *et al.* 2018; Hawk *et al.* 2018). The adaptation to new cultivation temperature involves transcriptional reconfiguration of genes expressed in the AFD thermosensory neurons (Yu *et al.* 2014). Our previous observations also indicated that *crh-1* is required to promote the adaptation to new cultivation temperature (Nishida *et al.* 2011). These findings thus suggest that the AFD neurons in *mec-2* mutants might be defective in setting the level of gene expression appropriate for the cultivation temperature. Since the AFD neurons apparently compute its neuronal outputs based on the cultivation temperature and current thermal context (Hawk *et al.* 2018; Nakano *et al.* 2020), such a defect in
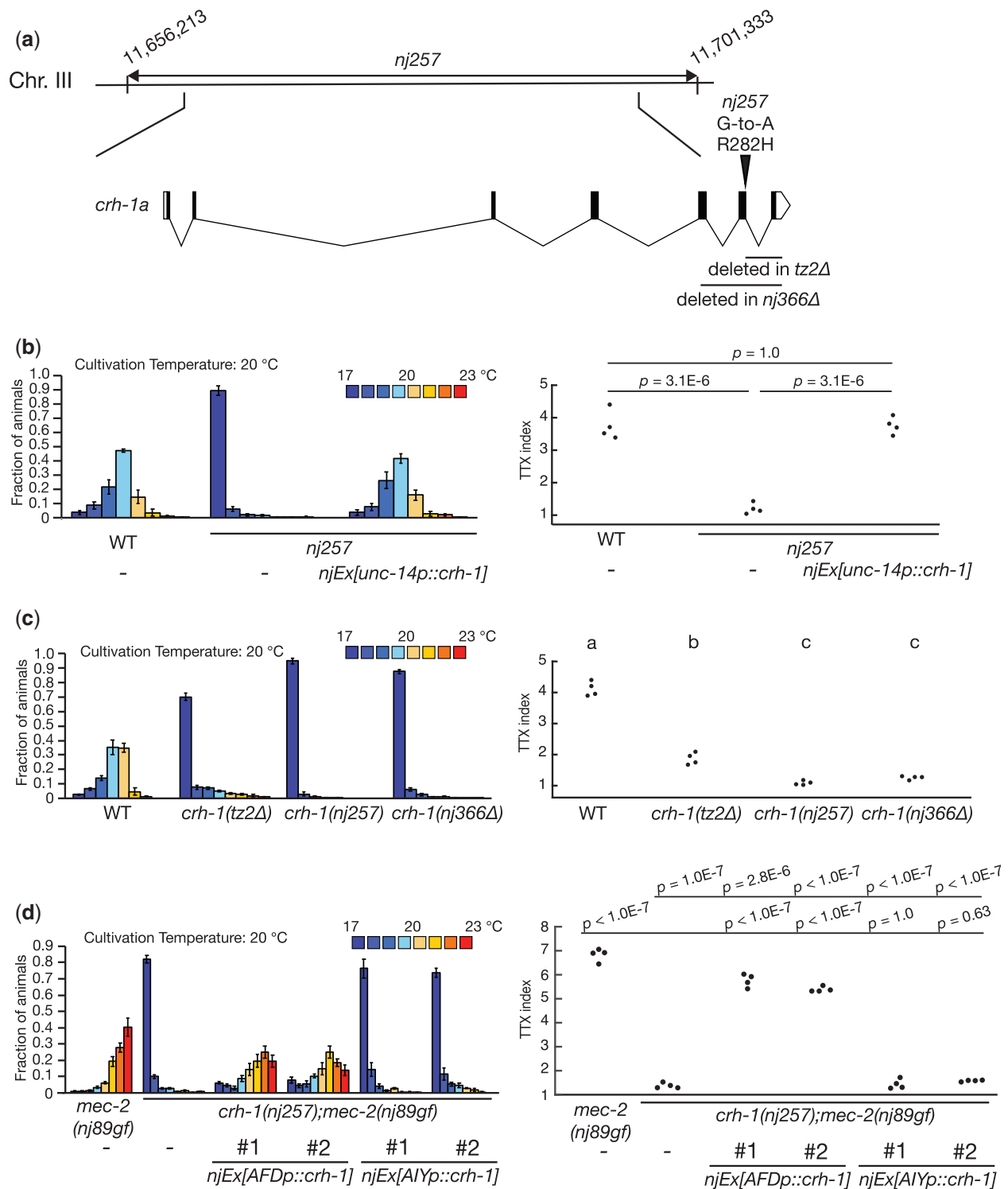
Fig. 8. *crh-1(nj257)* suppressed the thermophilic defect of *mec-2(nj89gf)*. (a) A chromosomal region to which *nj257* was mapped is indicated. The gene structure of *crh-1a* and mutations associated with each mutant are shown. The black boxes indicate exons, the lines introns, and the white boxes untranslated sequences. (b–d) Thermotaxis behaviors of *crh-1* mutants. Distributions of animals on the temperature gradients were shown as means ± SEM. TTX indices were indicated as dots. *P*-values were determined by 1-way ANOVA with Tukey–Kramer test.

AFD of *mec-2* mutants would result in an abnormal neuronal output from AFD, leading to a defect in the bidirectional AIY activity. Thus, in contrast to previous studies that indicated the roles of the stomatin family proteins in regulating the ion channels (Goodman *et al.* 2002; Price *et al.* 2004), our genetic screens suggest a new mode of the MEC-2/stomatin action that involves transcriptional regulation in controlling the dynamics of a neural circuitry.
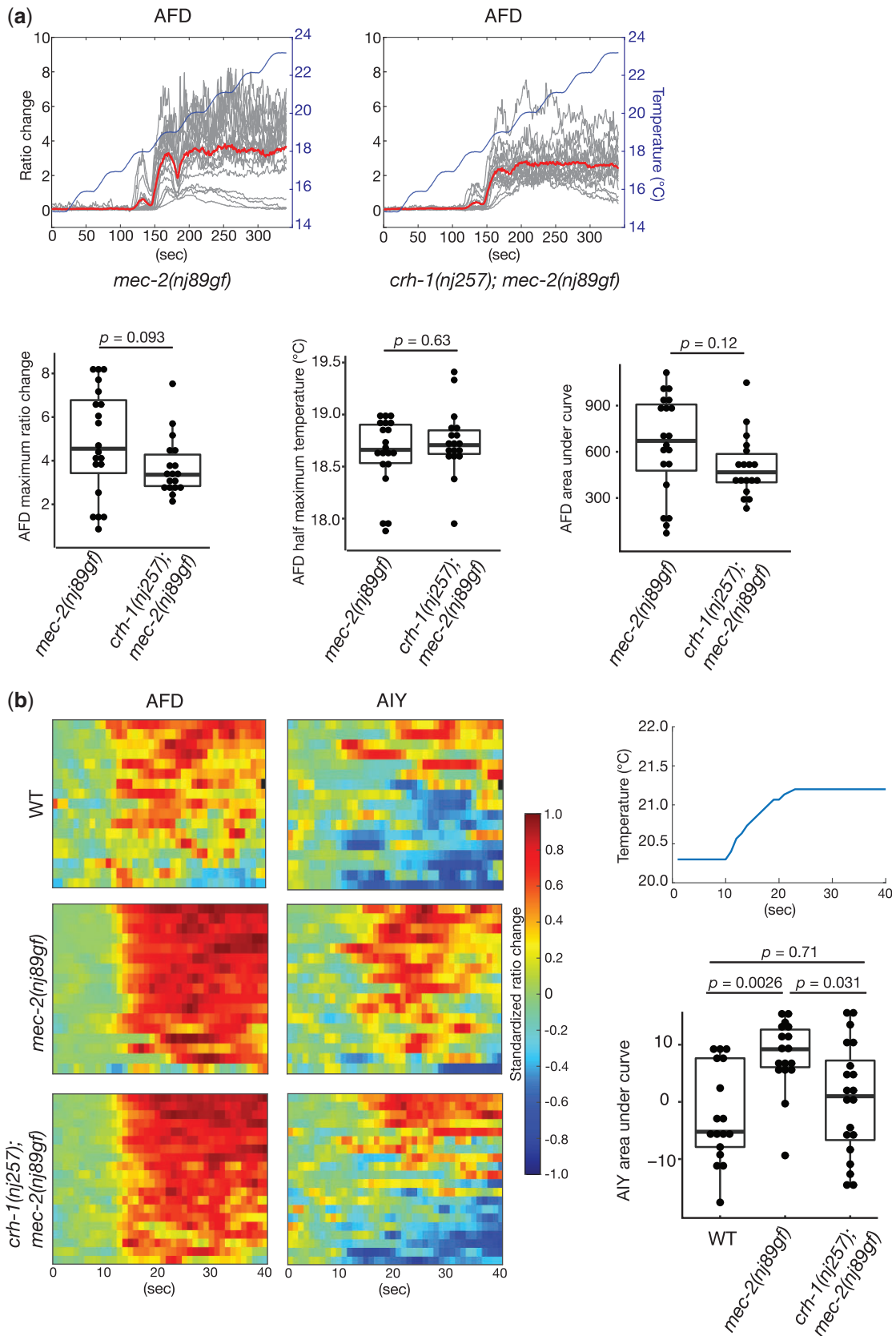
Fig. 9. *crh*-1 regulates the AIY neuronal activity. (a) Calcium imaging of the AFD thermosensory neurons in immobilized animals expressing the calcium indicator, YCX1.6. Animals were cultivated at 20°C. The temperature stimulus is shown in the blue lines. Individual calcium responses are shown as the ratio changes of YFP/CFP in gray lines. The mean responses are indicated in the red lines. The box and dot plots of the maximum ratio change, the half maximum temperature, and the area under the curve are shown. The boxes display the first and third quartiles, the lines inside the boxes are the medians, and the whiskers extend to 1.5-time interquartile range from the boxes. P-values were determined by Wilcoxon rank sum test for the comparisons of the maximum ratio change and the half maximum temperature and by student *t*-test for the area under the curve. *n* = 20 and 18 for *mec*-

(continued)

Data availability

Caenorhabditis elegans strains and plasmids are available upon request. Supplementary File 1 contains descriptions of the strains used in this study. Supplementary File 2 contains numeric data of imaging analyses from freely moving animals. Supplementary Files 3–10 contain the raw data of the thermotaxis assays shown in Figs. 1–8, respectively. The authors affirm that all data necessary for confirming the conclusions of the article are present within the article, figures, and supplemental materials. The custom scripts for the Ca^{2+} imaging analysis of freely moving animals are available from the GitHub at the following URL: https://github.com/ShunjiNakano/AIY_tracking.

Supplemental material is available at G3 online.

Conflicts of interest

None declared.

Literature cited

An SWA, Choi E-S, Hwang W, Son HG, Yang J-S, Seo K, Nam H-J, Nguyen NTH, Kim EJE, Suh BK, *et al.* KIN-4/MAST kinase promotes PTEN-mediated longevity of *Caenorhabditis elegans* via binding through a PDZ domain. Aging Cell. 2019;18(3):e12906. doi:10.1111/acel.12906.

Aoki I, Tateyama M, Shimomura T, Ihara K, Kubo Y, Nakano S, Mori I. SLO potassium channels antagonize premature decision making in *C. elegans*. Commun Biol. 2018;1:123. doi:10.1038/s42003-018-0124-5.

van Atteveldt N, Murray MM, Thut G, Schroeder CE. Multisensory integration: flexible use of general operations. Neuron. 2014;81(6):1240–1253. doi:10.1016/j.neuron.2014.02.044.

Beverly M, Anbil S, Sengupta P. Degeneracy and neuromodulation among thermosensory neurons contribute to robust thermosensory behaviors in *Caenorhabditis elegans*. J Neurosci. 2011;31(32):11718–11727. doi:10.1523/JNEUROSCI.1098-11.2011.

Brenner S. The genetics of *Caenorhabditis elegans*. Genetics. 1974;77(1):71–94. doi:10.1093/genetics/77.1.71.

Brose N, Betz A, Wegmeyer H. Divergent and convergent signaling by the diacylglycerol second messenger pathway in mammals. Curr Opin Neurobiol. 2004;14(3):328–340. doi:10.1016/j.conb.2004.05.006.

Chen Y-C, Chen H-J, Tseng W-C, Hsu J-M, Huang T-T, Chen C-H, Pan C-L. A *C. elegans* thermosensory circuit regulates longevity through *crh-1*/CREB-dependent *flp-6* neuropeptide signaling. Dev Cell. 2016;39(2):209–223. doi:10.1016/j.devcel.2016.08.021.

Clark DA, Biron D, Sengupta P, Samuel ADT. The AFD sensory neurons encode multiple functions underlying thermotactic behavior in *Caenorhabditis elegans*. J Neurosci. 2006;26(28):7444–7451. doi:10.1523/JNEUROSCI.1137-06.2006.

Clark DA, Gabel CV, Gabel H, Samuel ADT. Temporal activity patterns in thermosensory neurons of freely moving *Caenorhabditis elegans* encode spatial thermal gradients. J Neurosci. 2007;27(23):6083–6090. doi:10.1523/JNEUROSCI.1032-07.2007.

Cook SJ, Jarrell TA, Brittin CA, Wang Y, Bloniarz AE, Yakovlev MA, Nguyen KCQ, Tang LT-H, Bayer EA, Duerr JS, *et al.* Whole-animal connectomes of both *Caenorhabditis elegans* sexes. Nature. 2019;571(7763):63–71. doi:10.1038/s41586-019–1352-7.

Corbalán-García S, Gómez-Fernández JC. Classical protein kinases C are regulated by concerted interaction with lipids: the importance of phosphatidylinositol-4,5-bisphosphate. Biophys Rev. 2014;6(1):3–14. doi:10.1007/s12551-013–0125-z.

Dickinson DJ, Ward JD, Reiner DJ, Goldstein B. Engineering the *Caenorhabditis elegans* genome using Cas9-triggered homologous recombination. Nat Methods. 2013;10(10):1028–1034. doi:10.1038/nmeth.2641.

Dokshin GA, Ghanta KS, Piscopo KM, Mello CC. Robust genome editing with short single-stranded and long, partially single-stranded DNA donors in *Caenorhabditis elegans*. Genetics. 2018;210(3):781–787. doi:10.1534/genetics.118.301532.

Dunn FA, Rieke F. The impact of photoreceptor noise on retinal gain controls. Curr Opin Neurobiol. 2006;16(4):363–370. doi:10.1016/j.conb.2006.06.013.

Goodman MB, Ernstrom GG, Chelur DS, O'Hagan R, Yao CA, Chalfie M. MEC-2 regulates *C. elegans* DEG/ENaC channels needed for mechanosensation. Nature. 2002;415(6875):1039–1042. doi:10.1038/4151039a.

Hawk JD, Calvo AC, Liu P, Almoril-Porras A, Aljobeh A, Torruella-Suárez ML, Ren I, Cook N, Greenwood J, Luo L, *et al.* Integration of plasticity mechanisms within a single sensory neuron of *C. elegans* actuates a memory. Neuron. 2018;97(2):356–367.e4. doi:10.1016/j.neuron.2017.12.027.

Hedgecock EM, Russell RL. Normal and mutant thermotaxis in the nematode *Caenorhabditis elegans*. Proc Natl Acad Sci U S A. 1975;72(10):4061–4065. doi:10.1073/pnas.72.10.4061.

Hiroki S, Yoshitane H, Mitsui H, Sato H, Umatani C, Kanda S, Fukada Y, Iino Y. Molecular encoding and synaptic decoding of context during salt chemotaxis in *C. elegans*. Nat Commun. 2022;13(1):2928. doi:10.1038/s41467-022–30279-7.

Hobert O, Mori I, Yamashita Y, Honda H, Ohshima Y, Liu Y, Ruvkun G. Regulation of interneuron function in the *C. elegans* thermoregulatory pathway by the *ttx-3* LIM homeobox gene. Neuron. 1997;19(2):345–357. doi:10.1016/s0896-6273(00)80944-7.

Fig. 9. Continued

2(nj89gf) and *crh-1(nj257)*; *mec-2(nj89gf)* animals, respectively. (b) Calcium imaging from freely moving animals expressing YCX1.6 in the AFD and AIY neurons. Animals were cultivated at 20°C. The heatmaps indicate the standardized ratio change of the AFD and AIY calcium dynamics. The baseline standardized ratio change, which corresponds to the mean of the standardized ratio changes for the first 10 s, was subtracted from the standardized ratio change of each frame. A representative of the temperature stimulus is shown. The areas under the curve of the AIY standardized ratio changes were calculated for the time after the temperature increase was applied and were shown in the box and dot plots. The boxes indicate the first and third quartiles, the lines inside the boxes are the medians, and the whiskers extend to 1.5-time interquartile range from the boxes. *P*-values were determined by Steel–Dwass test. $n = 17$, 17, and 20 for the wild-type, *mec-2(nj89gf)* and *crh-1(nj257)*; *mec-2(nj89gf)* animals, respectively.

Huang M, Gu G, Ferguson EL, Chalfie M. A stomatin-like protein necessary for mechanosensation in *C. elegans*. Nature. 1995; 378(6554):292–295. doi:10.1038/378292a0.

Ikeda M, Nakano S, Giles AC, Xu L, Costa WS, Gottschalk A, Mori I. Context-dependent operation of neural circuits underlies a navigation behavior in *Caenorhabditis elegans*. Proc Natl Acad Sci U S A. 2020;117(11):6178–6188. doi:10.1073/pnas.1918528117.

Ito H, Inada H, Mori I. Quantitative analysis of thermotaxis in the nematode *Caenorhabditis elegans*. J Neurosci Methods. 2006; 154(1–2):45–52. doi:10.1016/j.jneumeth.2005.11.011.

Kato S, Kaplan HS, Schrödel T, Skora S, Lindsay TH, Yemini E, Lockery S, Zimmer M. Global brain dynamics embed the motor command sequence of *Caenorhabditis elegans*. Cell. 2015;163(3): 656–669. doi:10.1016/j.cell.2015.09.034.

Kimura KD, Miyawaki A, Matsumoto K, Mori I. The *C. elegans* thermosensory neuron AFD responds to warming. Curr Biol. 2004;14(14): 1291–1295. doi:10.1016/j.cub.2004.06.060.

Kimura Y, Corcoran EE, Eto K, Gengyo-Ando K, Muramatsu M-A, Kobayashi R, Freedman JH, Mitani S, Hagiwara M, Means AR, *et al.* A CaMK cascade activates CRE-mediated transcription in neurons of *Caenorhabditis elegans*. EMBO Rep. 2002;3(10):962–966. doi: 10.1093/embo-reports/kvf191.

Kobayashi K, Nakano S, Amano M, Tsuboi D, Nishioka T, Ikeda S, Yokoyama G, Kaibuchi K, Mori I. Single-cell memory regulates a neural circuit for sensory behavior. Cell Rep. 2016;14(1):11–21. doi:10.1016/j.celrep.2015.11.064.

Kuhara A, Okumura M, Kimata T, Tanizawa Y, Takano R, Kimura KD, Inada H, Matsumoto K, Mori I. Temperature sensing by an olfactory neuron in a circuit controlling behavior of *C. elegans*. Science. 2008;320(5877):803–807. doi:10.1126/science.1148922.

Kunitomo H, Sato H, Iwata R, Satoh Y, Ohno H, Yamada K, Iino Y. Concentration memory-dependent synaptic plasticity of a taste circuit regulates salt concentration chemotaxis in *Caenorhabditis elegans*. Nat Commun. 2013;4(1):2210. doi:10.1038/ncomms3210.

Land M, Rubin CS. A calcium- and diacylglycerol-stimulated protein kinase C (PKC), *Caenorhabditis elegans* PKC-2, links thermal signals to learned behavior by acting in sensory neurons and intestinal cells. Mol Cell Biol. 2017;37(19):e00192–17. doi:10.1128/MCB.00192-17.

Li Z, Liu J, Zheng M, Xu XZS. Encoding of both analog- and digital-like behavioral outputs by one *C. elegans* interneuron. Cell. 2014; 159(4):751–765. doi:10.1016/j.cell.2014.09.056.

Luo L, Cook N, Venkatachalam V, Martinez-Velazquez LA, Zhang X, Calvo AC, Hawk J, MacInnis BL, Frank M, Ng JHR, *et al.* Bidirectional thermotaxis in *Caenorhabditis elegans* is mediated by distinct sensorimotor strategies driven by the AFD thermosensory neurons. Proc Natl Acad Sci U S A. 2014;111(7):2776–2781. doi:10.1073/pnas.1315205111.

Madisen L, Garner AR, Shimaoka D, Chuong AS, Klapoetke NC, Li L, van der Bourg A, Niino Y, Egolf L, Monetti C, *et al.* Transgenic mice for intersectional targeting of neural sensors and effectors with high specificity and performance. Neuron. 2015;85(5):942–958. doi:10.1016/j.neuron.2015.02.022.

Mathis A, Mamidanna P, Cury KM, Abe T, Murthy VN, Mathis MW, Bethge M. DeepLabCut: markerless pose estimation of user-defined body parts with deep learning. Nat Neurosci. 2018;21(9): 1281–1289. doi:10.1038/s41593-018–0209-y.

Mello CC, Kramer JM, Stinchcomb D, Ambros V. Efficient gene transfer in *C. elegans*: extrachromosomal maintenance and integration of transforming sequences. EMBO J. 1991;10(12):3959–3970. doi: 10.1002/j.1460–2075.1991.tb04966.x.

Mohri A, Kodama E, Kimura KD, Koike M, Mizuno T, Mori I. Genetic control of temperature preference in the nematode *Caenorhabditis elegans*. Genetics. 2005;169(3):1437–1450. doi:10.1534/genetics.104.036111.

Mori I, Ohshima Y. Neural regulation of thermotaxis in *Caenorhabditis elegans*. Nature. 1995;376(6538):344–348. doi:10.1038/376344a0.

Nakano S, Ikeda M, Tsukada Y, Fei X, Suzuki T, Niino Y, Ahluwalia R, Sano A, Kondo R, Ihara K, *et al.* Presynaptic MAST kinase controls opposing postsynaptic responses to convey stimulus valence in *Caenorhabditis elegans*. Proc Natl Acad Sci U S A. 2020;117(3): 1638–1647. doi:10.1073/pnas.1909240117.

Nath T, Mathis A, Chen AC, Patel A, Bethge M, Mathis MW. Using DeepLabCut for 3D markerless pose estimation across species and behaviors. Nat Protoc. 2019;14(7):2152–2176. doi: 10.1038/s41596-019–0176-0.

Nishida Y, Sugi T, Nonomura M, Mori I. Identification of the AFD neuron as the site of action of the CREB protein in *Caenorhabditis elegans* thermotaxis. EMBO Rep. 2011;12(8):855–862. doi:10.1038/embor.2011.120.

Ohno H, Sakai N, Adachi T, Iino Y. Dynamics of presynaptic diacylglycerol in a sensory neuron encode differences between past and current stimulus intensity. Cell Rep. 2017;20(10):2294–2303. doi:10.1016/j.celrep.2017.08.038.

Okochi Y, Kimura KD, Ohta A, Mori I. Diverse regulation of sensory signaling by *C. elegans* nPKC-epsilon/eta TTX-4. EMBO J. 2005; 24(12):2127–2137. doi:10.1038/sj.emboj.7600697.

Price MP, Thompson RJ, Eshcol JO, Wemmie JA, Benson CJ. Stomatin modulates gating of acid-sensing ion channels. J Biol Chem. 2004; 279(51):53886–53891. doi:10.1074/jbc.M407708200.

Ramot D, MacInnis BL, Goodman MB. Bidirectional temperature-sensing by a single thermosensory neuron in *C. elegans*. Nat Neurosci. 2008;11(8):908–915. doi:10.1038/nn.2157.

Sato H, Kunitomo H, Fei X, Hashimoto K, Iino Y. Glutamate signaling from a single sensory neuron mediates experience-dependent bidirectional behavior in *Caenorhabditis elegans*. Cell Rep. 2021;35(8): 109177. doi:10.1016/j.celrep.2021.109177.

Takeishi A, Yu YV, Hapiak VM, Bell HW, O'Leary T, Sengupta P. Receptor-type guanylyl cyclases confer thermosensory responses in *C. elegans*. Neuron. 2016;90(2):235–244. doi:10.1016/j.neuron.2016.03.002.

Tsukada Y, Yamao M, Naoki H, Shimowada T, Ohnishi N, Kuhara A, Ishii S, Mori I. Reconstruction of spatial thermal gradient encoded in thermosensory neuron AFD in *Caenorhabditis elegans*. J Neurosci. 2016;36(9):2571–2581. doi:10.1523/JNEUROSCI.2837-15.2016.

Walden PD, Cowan NJ. A novel 205-kilodalton testis-specific serine/threonine protein kinase associated with microtubules of the spermatid manchette. Mol Cell Biol. 1993;13(12):7625–7635. doi: 10.1128/mcb.13.12.7625–7635.1993.

White JG, Southgate E, Thomson JN, Brenner S. The structure of the nervous system of the nematode *Caenorhabditis elegans*. Philos Trans R Soc Lond B Biol Sci. 1986;314(1165):1–340. doi:10.1098/rstb.1986.0056.

Yoshida A, Nakano S, Suzuki T, Ihara K, Higashiyama T, Mori I. A glial K+/Cl− cotransporter modifies temperature-evoked dynamics in *Caenorhabditis elegans* sensory neurons. Genes Brain Behav. 2016;15(4):429–440. doi:10.1111/gbb.12260.

Yu YV, Bell HW, Glauser D, Van Hooser SD, Goodman MB, Sengupta P. CaMKI-dependent regulation of sensory gene expression mediates experience-dependent plasticity in the operating range of a thermosensory neuron. Neuron. 2014;84(5):919–926. doi:10.1016/j.neuron.2014.10.046.

Communicating editor: R. Anholt